Langmuir

Article

pubs.acs.org/Langmuir

Low-Cost Synthesis of Flowerlike α-Fe_2O_3 Nanostructures for Heavy Metal Ion Removal: Adsorption Property and Mechanism

Chang-Yan Cao,[†] Jin Qu,[†] Wen-Sheng Yan,[‡] Jun-Fa Zhu,[‡] Zi-Yu Wu,[‡] and Wei-Guo Song*[,†]

[†]Beijing National Laboratory for Molecular Science (BNLMS), Laboratory of Molecular Nanostructures and Nanotechnology, Institute of Chemistry, Chinese Academy of Sciences, Beijing 100190, People's Republic of China

[‡]National Synchrotron Radiation Laboratory, University of Science and Technology of China, Hefei 230029, People's Republic of China

Supporting Information

ABSTRACT: Flowerlike α-Fe_2O_3 nanostructures were synthesized via a template-free microwave-assisted solvothermal method. All chemicals used were low-cost compounds and environmentally benign. These flowerlike α-Fe_2O_3 nanostructures had high surface area and abundant hydroxyl on their surface. When tested as an adsorbent for arsenic and chromium removal, the flowerlike α-Fe_2O_3 nanostructures showed excellent adsorption properties. The adsorption mechanism for As^V and Cr^{VI} onto flowerlike α-Fe_2O_3 nanostructures was elucidated by X-ray photoelectron spectroscopy and synchrotron-based X-ray absorption near edge structure analysis. The results suggested that ion exchange between surface hydroxyl groups and As^V or Cr^{VI} species was accounted for by the adsorption. With maximum capacities of 51 and 30 mg g^{-1} for As^V and Cr^{VI}, respectively, these low-cost flowerlike α-Fe_2O_3 nanostructures are an attractive adsorbent for the removal of As^V and Cr^{VI} from water.

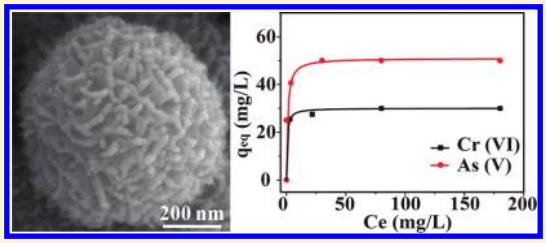

1. INTRODUCTION

Recently, the exploitation of iron oxide nanomaterials for heavy metal ion removal has attracted attention because of their demonstrated excellent adsorption capacities and environmentally benign nature.[1−5] Among various morphologies of α-Fe_2O_3 nanomaterials, three-dimensional (3D) flowerlike nanostructures composed of hierarchically assembled nanosized building blocks, with the total size in the micrometer scale, have several advantages for adsorption, such as high surface area, easy mass transformation, and easy separation.[3,6−8] However, it is quite expensive to produce flowerlike α-Fe_2O_3 nanomaterials using a popular ethylene glycol (EG)-mediated process. In our previous study, flowerlike α-Fe_2O_3 nanostructures were prepared through heating iron chloride and urea in EG at 180 °C for several hours, using tetrabutylammonium bromide (TBAB) as the surfactant, followed by calcination.[3] This EG-mediated method is a simple and reliable synthetic method to produce hierarchically self-assembled flowerlike α-Fe_2O_3 architectures but consumes EG and TBAB because it may be even more expensive to recycle them, making it difficult to use flowerlike α-Fe_2O_3 in practical water treatment. Thus, it is very desirable to develop a low-cost method to produce flowerlike α-Fe_2O_3 nanomaterials. In general, the material cost can be lowered using low-cost raw materials, shortening the heating time, and recycling unused materials.

In addition, the adsorption mechanisms of flowerlike α-Fe_2O_3 nanostructures for heavy metal ions, such as As^V and Cr^{VI}, were believed to involve electrostatic attraction and/or ion exchange.[1,3,5,9] However, how ion exchange occurred, i.e., what species are involved in the process, and how heavy metal ions are bound to the adsorbent remain not very clear. For the rational design of materials, such knowledge is also needed.

In this study, we developed a surfactant-free microwave-assisted solvothermal method to prepare flowerlike α-Fe_2O_3 nanostructures. All chemicals ($FeCl_3{\cdot}6H_2O$ and urea as reaction materials and ethanol as the solvent and can be recycled) used were low-cost and environmentally benign. The reaction time was less than 30 min with microwave heating. These make this route a rapid, reliable, and easily scaled-up method. These flowerlike α-Fe_2O_3 nanostructures had a large surface area (130 m^2 g^{-1}) and abundant surface hydroxyl groups and showed excellent adsorption properties for As^V and Cr^{VI}. The maximum adsorption capacities for As^V and Cr^{VI} were 51 and 30 mg g^{-1}, respectively. These values were nearly 170 times higher than that of the commercial bulk α-Fe_2O_3. The high surface area as well as abundant surface hydroxyl groups accounted for the excellent adsorption properties of flowerlike α-Fe_2O_3 nanostructures. X-ray photoelectron spectroscopy (XPS) and synchrotron-based X-ray absorption near edge structure (XANES) analysis showed unambiguous evidence to support an ion-exchange adsorption mechanism between hydroxyl on the surface of flowerlike α-Fe_2O_3 nanostructures and As^V and Cr^{VI} species in the solution during adsorption.

Received: January 6, 2012
Revised: February 8, 2012
Published: February 9, 2012

   dx.doi.org/10.1021/la300097y | *Langmuir* 2012, 28, 4573−4579

2. EXPERIMENTAL SECTION

2.1. Preparation of Flowerlike α-Fe_2O_3 Nanostructures. All of the materials, including iron(III) chloride hexahydrate ($FeCl_3{\cdot}6H_2O$), urea, and ethanol, were used as received from Beijing Chemicals Co. (Beijing, China). In a typical procedure, 5 mmol of $FeCl_3{\cdot}6H_2O$ and 7.5 mmol of urea were dissolved in 100 mL of anhydrous ethanol (99%), and then 40 mL of reaction solution was poured into a Teflon-lined autoclave with a volume of 70 mL. The autoclave was sealed and place in a programmable microwave oven (MDS-6, Shanghai Sineo Microwave Chemistry Technology Co., Ltd.). The oven was heated to 150 °C in 2 min by microwave irradiation and then kept at that temperature for another 30 min under microwave heating. After cooling to room temperature, precipitates were collected as α-Fe_2O_3 by centrifugation, washed with ethanol 5 times, and then dried at 80 °C for 3 h.

2.2. Characterizations. X-ray diffraction (XRD) patterns were preformed on a Rigaku D/max-2500 diffractometer with Cu Kα radiation (λ = 1.5418 Å) at 40 kV and 200 mA. The morphology and microstructures of the samples were characterized by field emission scanning electron microscopy (FE-SEM, JEOL 6701F), transmission electron microscopy (TEM, JEOL 1011), and high-resolution transmission electron microscopy (HR-TEM) (FEI Tecnai F20). The nitrogen adsorption−desorption isotherms were measured on a Quantachrome Autosorb AS-1 instrument. The pore size distributions were derived from the desorption branches using the Barrett−Joyner−Halenda (BJH) model. XPS data were obtained with an ESCALab220i-XL electron spectrometer from VG Scientific using 300 W Al Kα radiation. The binding energies were referenced to the C 1s line at 284.8 eV from adventitious carbon. Fourier transform infrared (FTIR) spectroscopy was characterized on Bruker Tensor 27. Samples were dried before characterization by an infrared lamp to remove the adsorbed water. Synchrotron-based XANES experiments were performed on the soft X-ray magnetic circular dichroism (SXMCD) station at the National Synchrotron Radiation Laboratory (NSRL) in Hefei, China. The samples were loaded in an ultrahigh-vacuum chamber at a vacuum of 3×10^{-9} Pa. All spectra were acquired in the total electron yield (TEY) mode with an experimental resolution of 0.2 eV at room temperature.

2.3. Heavy Metal Ion Adsorption. Solutions with different concentrations of As^V and Cr^{VI} were prepared using $Na_2HAsO_4{\cdot}7H_2O$ and $K_2Cr_2O_7$ as the sources of heavy metal ions, respectively. The pH value was adjusted to 3 using HCl (2 M). For the adsorption kinetic study of As^V, 20 mg of flowerlike α-Fe_2O_3 was added to 50 mL solutions with an As^V initial concentration of 25 mg L^{-1}, while 20 mg of adsorbent was added to 30 mL solutions with a Cr^{VI} initial concentration of 25 mg L^{-1}. After a specified time, the solid and liquid were separated immediately and analyzed by inductively coupled plasma−optical emission spectroscopy (Shimazu ICPE-9000) to measure the concentration of metal ions in the remaining solution. For the adsorption isothermal study, 20 mg of adsorbent was added to 50 mL of solution with different concentrations under stirring for 12 h at room temperature.

3. RESULTS AND DISCUSSION

3.1. Characterizations of Flowerlike α-Fe_2O_3 Nanostructures. Flowerlike α-Fe_2O_3 nanostructures were produced using iron chloride and urea as raw materials and ethanol as the solvent. All chemicals used were low-cost chemicals and environmentally benign. Unlike previously reported EG-mediated methods for flowerlike nanostructures,[3,10−12] no organic template or organic metal compounds were used. In addition, notably, α-Fe_2O_3 nanostructures were directly produced without calcinations. In the EG-mediated process, iron-alkoxide-type compounds were first produced and then converted into iron oxide by calcination, which is time-consuming and costly.[3]

The typical SEM image of the obtained sample was shown in Figure 1a. They were composed of many uniform, flowerlike

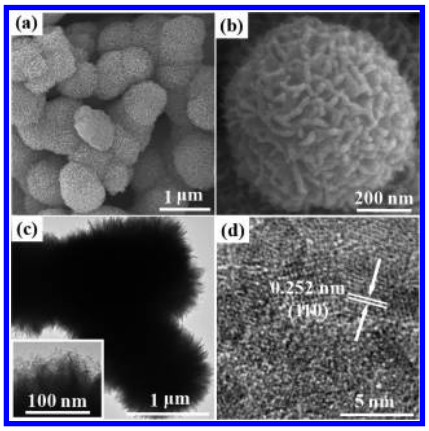

Figure 1. (a) Low-magnification SEM image, (b) high-magnification SEM image, (c) TEM image (inset: high-magnification TEM image), and (d) HR-TEM image of flowerlike α-Fe_2O_3 nanostructures.

architectures approximately 0.8−1 μm in diameter. The flowerlike α-Fe_2O_3 nanostructures in this study were composed of hundreds of small petals, making the surface of the overall structure uniform. This is quite different from the one in our previous study, which was composed of a large but small number of petal-like leaves.[3] A high-magnification SEM image (Figure 1b) revealed that the entire structure were built of many nanopetals and connected to each other to form 3D flowerlike structures. The TEM image (Figure 1c) further confirmed the hierarchical flowerlike structures. Nanoparticals were self-assembled to form nanopetals, which were then self-assembled to form flowerlike nanostructures. A representative high-resolution TEM (HR-TEM) image taken from α-Fe_2O_3 nanoparticles was shown in Figure 1d. Lattice fringes from nanoparticles were clearly visible, with a spacing of 0.252 nm, corresponding to the spacing of the (110) planes of α-Fe_2O_3.

The powder XRD pattern of the typical sample obtained was shown in Figure 2a. The diffraction peaks can be indexed to the hexagonal phase of α-Fe_2O_3 [Joint Committee on Powder Diffraction Standards (JCPDS) 80-2377], which was in good agreement with the HR-TEM result. The energy-dispersive spectrometry (EDS) spectrum also showed that only Fe and O elements exsited in the sample (see Figure S1 of the Supporting Information).

The surface area and pore size distribution of flowerlike α-Fe_2O_3 nanostructures were tested by nitrogen adsorption−desorption (Figure 2b). The Brunauer−Emmett−Teller (BET) surface area of flowerlike α-Fe_2O_3 nanostructures was calculated to be 130 m^2 g^{-1}. This was a very high surface area for iron oxide hierarchical flowerlike nanostructures. Such a surface area value is equivalent to α-Fe_2O_3 nanoparticles of 4.4 nm based on the equivalent average particle size calculation.[13,14] There was a sharp pore distribution with an average diameter of 3.7 nm obtained by the BJH method. These pores were likely due to the void space of self-assembled nanoparticles.

The yield of flowerlike α-Fe_2O_3 nanostructures was nearly 100% based on the amount of $FeCl_3{\cdot}6H_2O$. The crystal water in $FeCl_3{\cdot}6H_2O$ was actually an essential part of the following reaction sequences. Both hydrolysis of urea and formation of $Fe(OH)_3$ need water, and the concentration of water

dx.doi.org/10.1021/la300097y | Langmuir 2012, 28, 4573−4579

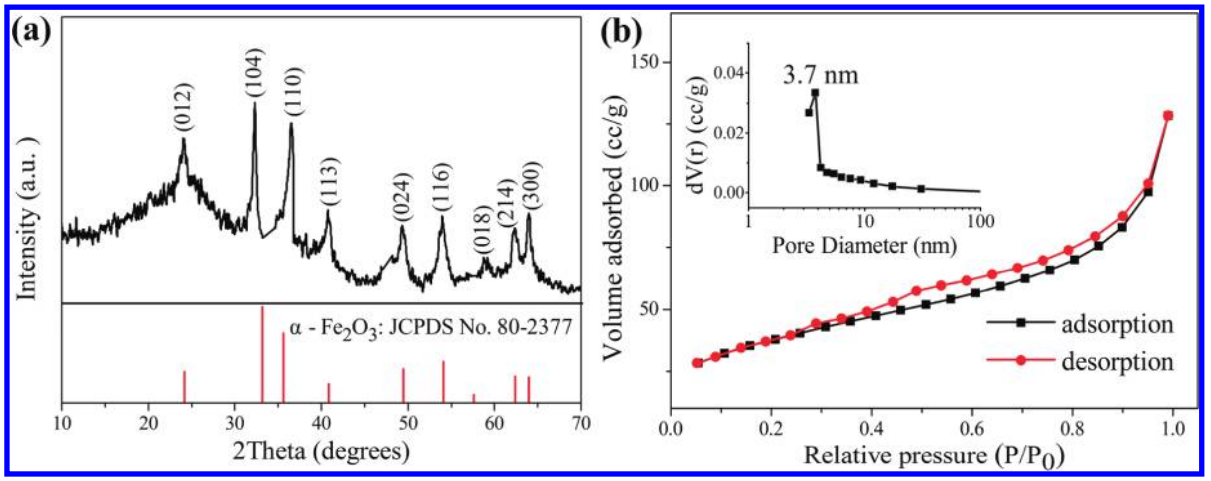

Figure 2. (a) XRD pattern and (b) N_2 adsorption−desorption isothermals (inset: pore size distribution) of flowerlike α-Fe_2O_3 nanostructures.

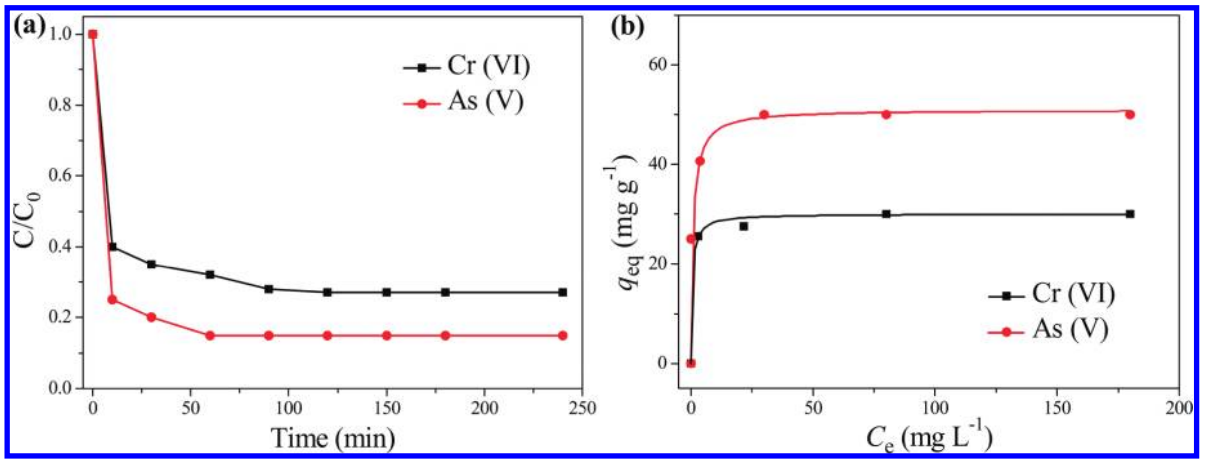

Figure 3. (a) Adsorption rate curves (initial concentration of 25 mg L^{-1}) and (b) adsorption isotherms of As^V and Cr^{VI} using flowerlike α-Fe_2O_3 nanostructures.

determined the rate of these two steps. Flowerlike nanostructures could be produced only within a narrow range of the water content. When anhydrous $FeCl_3$ was used instead of $FeCl_3{\cdot}6H_2O$, only irragular aggregate particles were obtained (see Figure S2a of the Supporting Information). When the water content exceeded 0.5%, only aggregated nanoparticles were obtained again (see Figure S2b of the Supporting Information).

The role of urea was to provide steady but low concentrations of the OH^- group for Fe^{III} to form $Fe(OH)_3$. On the basis of the following reaction sequences, the stochiochemical ratio of urea and $FeCl_3{\cdot}6H_2O$ should be 1:1.5 (mole ratio). In this study, we found that, as long as the amount of urea was no less than the stochiochemical requirement, flowerlike α-Fe_2O_3 nanostructures were produced. Thus, the simplest and lowest cost recipe was to use a stochiochemical amount of urea and $FeCl_3{\cdot}6H_2O$.

$$CO(NH_2)_2 + H_2O \rightarrow 2NH_3 + CO_2 \quad (1)$$

$$NH_3 + H_2O \rightarrow NH^{4+} + OH^- \quad (2)$$

$$Fe^{3+} + 3OH^- \rightarrow Fe(OH)_3 \quad (3)$$

$$NH^{4+} + Cl^- \rightarrow NH_4Cl \quad (4)$$

Ethanol was not consumed during the synthesis. It could be recycled after fast distillation to remove the ammonia-related species, which somehow led to irregular-shaped particles if ethanol was directly reused. As shown in Figure S2c of the Supporting Information, the morphology of the flowerlike α-Fe_2O_3 nanostructures obtained from recycled ethanol was the same as that using fresh ethanol.

3.2. Heavy Metal Ion Adsorption Property. Clean water, especially free of highly toxic heavy metal ions, is vital to people's health. Considerable attention has been paid to the water treatment in recent years.[15,16] Among all of the heavy metal ion removal methods, the adsorption technique is perhaps the most extensively adopted method because of its simplicity and low cost.[17−22] Nanomaterial sorbents showed higher adsorption properties than bulk materials because of the nanosize effects. This may provide an efficient way to help solve the water problem. Because of their 3D hierarchical and porous structure, we expected that these flowerlike α-Fe_2O_3 nanostructures would be useful in heavy metal ion adsorption. In addition, the large surface area may be beneficial for mass transformation and adsorption. Because the total size of flowerlike α-Fe_2O_3 nanostructures was in micrometers, the separation would be fairly easy.

Arsenic and chromium are two typical toxic heavy metal ions in water resources, one from natural causes and the other from industrial emissions, and their efficient removal is of great

dx.doi.org/10.1021/la300097y | Langmuir 2012, 28, 4573−4579

importance. Figure 3a showed the adsorption rates of As^V and Cr^{VI} ions with an inititial concentration of 25 mg L^{-1} on the flowerlike α-Fe_2O_3 nanostructure samples. The adsorption processes were very fast during the first 30 min, and the equilibrium were established after 3 h. To further investigate the adsorption property, adsorption isotherms were obtained with different initial concentrations ranging from 10 to 200 mg L^{-1}, as shown in Figure 3b. Experimental data were fitted well with the Langmuir adsorption model isotherm, from which the maximum adsorption capacity could be calculated.[11,23] The maximum adsorption capacity of flowerlike α-Fe_2O_3 nanostructures was 51 mg g^{-1} for As^V and 30 mg g^{-1} for Cr^{VI}. These values were much higher than those flowerlike α-Fe_2O_3,[3] flowerlike CeO_2[10] and hollow CeO_2 nanostructures[11] in our previous studies and nearly about 170 times higher than that of commercial bulk α-Fe_2O_3, as shown in Table 1. In addition,

Table 1. BET Surface Area and Maximum Adsorption Capacity for As^V and Cr^{VI} at the Same Experimental Conditions

adsorbent sample	BET surface area (m^2 g^{-1})	maximum adsorption capacity	
		As^V (mg g^{-1})	Cr^{VI} (mg g^{-1})
flowerlike α-Fe_2O_3 (this study)	130	51	30
CeO_2 hollow nanospheres[11]	72	22.4	15.4
flowerlike CeO_2[10]	34	14.4	5.9
flowerlike α-Fe_2O_3[3]	40	7.6	5.4
commercial α-Fe_2O_3	2	0.3	0.37

TEM images showed that the morphology of flowerlike α-Fe_2O_3 nanostructures was not changed after adsorption of As^V and Cr^{VI} ions (see Figure S3 of the Supporting Information)

$$q_e = q_m b C_e/(1 + bC_e)$$

where C_e is the equilibrium concentration of heavy metal ions (mg L^{-1}), q_e is the amount of heavy metal ions adsorbed per unit weight of the adsorbent at equilibrium (mg/g), q_m (mg/g) is the maximum adsorption capacity, and b is the equilibrium constant related to the energy.

3.3. Adsorption Mechanism. To investigate the adsorption mechanism for heavy metal ions, As^V- and Cr^{VI}-saturated flowerlike α-Fe_2O_3 nanostructures were prepared. As^V and Cr^{VI} ions exsited perdominately as $H_2AsO_4^-$ and $Cr_2O_7^{2-}/HCrO_4^-$ in aqueous solution with pH 3, and the surface of flowerlike α-Fe_2O_3 was positively charged. Therefore, the electrostatic attraction between positively charged α-Fe_2O_3 samples and negatively charged As^V and Cr^{VI} species was the initial driving force to bind the anions onto the surface. EDS confirmed that As^V and Cr^{VI} ions were adsorbed on the flowerlike α-Fe_2O_3 nanostructures. As shown in panels a and b of Figure 4, As and Cr elements were observed in the EDS spectra. The element mapping (see panels a and b of Figure S4 of the Supporting Information) indicated that As and Cr were evenly distributed on the surface of flowerlike α-Fe_2O_3 nanostructures.

The adsorption mainly occurred on the surface. Therefore, XPS was used to characterize the surface states of flowerlike α-Fe_2O_3 nanostructures before and after adsorption of heavy metal ions. Figure 5a showed full-range XPS spectra of flowerlike α-Fe_2O_3 nanostructures before and after As^V and Cr^{VI} adsorption. As and Cr information appeared after As^V and Cr^{VI} were adsorbed on flowerlike α-Fe_2O_3 nanostructures. The As 3d spectrum after As^V adsorption (see Figure S5a of the Supporting Information) showed a peak located at 45.4 eV, which should be attributed to As^V−O bonding.[24] The Cr 2p spectrum after Cr^{VI} adsorption (see Figure S5b of the Supporting Information) showed two peaks located at 579.5 and 588.7 eV, which can be attributed to Cr $2p_{3/2}$−O and Cr $2p_{1/2}$−O bonding, respectively.[25] All of these results indicated that As^V and Cr^{VI} were adsorbed on the surface of flowerlike α-Fe_2O_3 nanostructures.

A high-resolution O 1s XPS spectrum of flowerlike α-Fe_2O_3 (Figure 5b) can be deconvoluted into peaks located at 530.0 and 531.5 eV, which can be attributed to oxygen in the lattice, i.e., oxygen atoms that were bound to only iron atoms (Fe−O), and oxygen atoms on the surface, i.e., oxygen atoms in surface hydroxyl groups (H−O), respectively. The peak intensity of H−O species was significantly higher than that of Fe−O, confirming that there were many hydroxyl groups on the surface of fresh flowerlike α-Fe_2O_3. However, the binding energy of the O 1s shifts to low energy after As^V and Cr^{VI} adsorption, as shown in panels c and d of Figure 5, respectively. The intensity of the H−O peak became lower than that of the

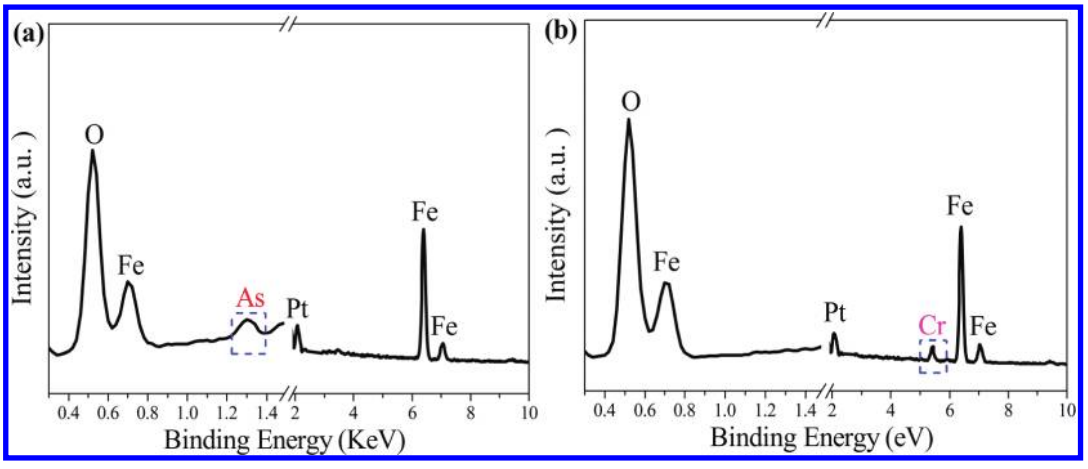

Figure 4. EDS spectra of flowerlike α-Fe_2O_3 after adsorption of heavy metal ions: (a) As^V adsorption and (b) Cr^{VI} adsorption (break peaks were attributed to Si).

dx.doi.org/10.1021/la300097y | Langmuir 2012, 28, 4573−4579

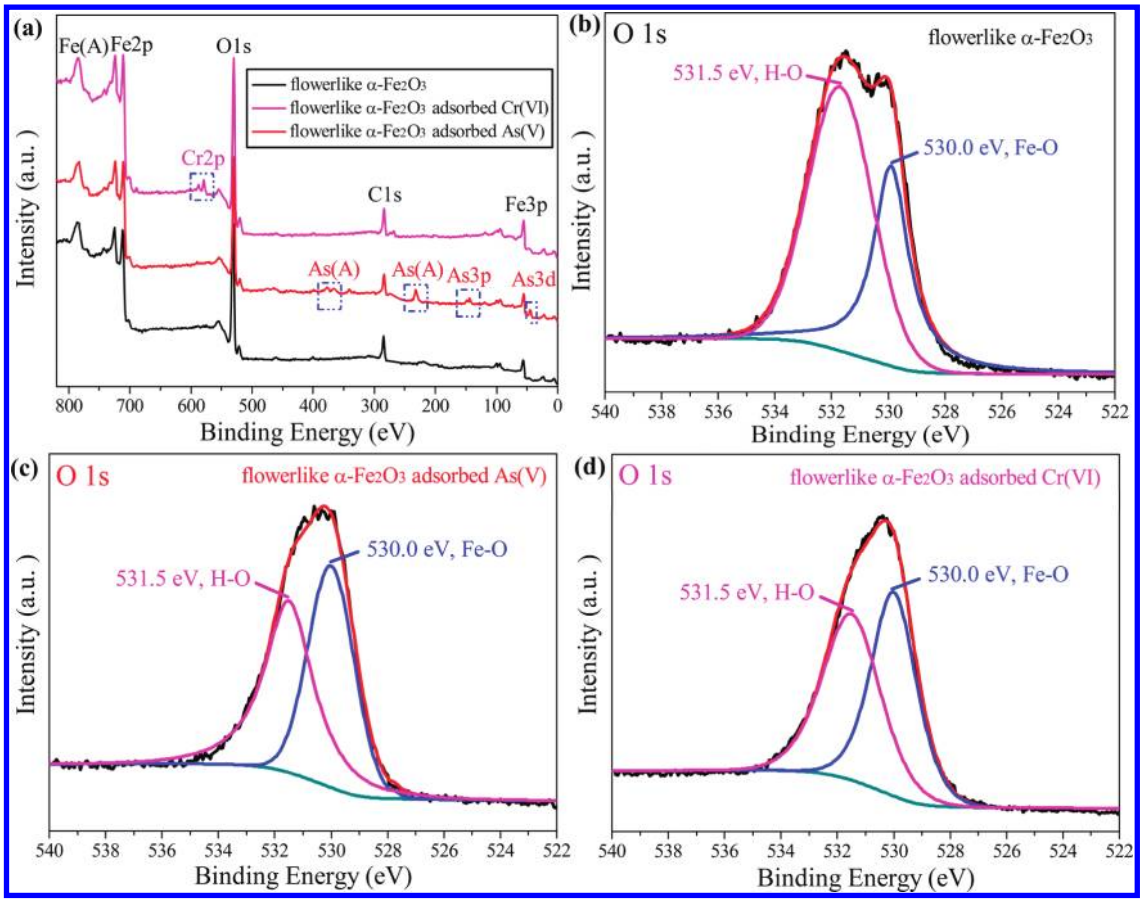

Figure 5. (a) Full-range XPS spectra of flowerlike α-Fe_2O_3 nanostructures and after As^V and Cr^{VI} adsorption. (b) O 1s XPS spectrum of flowerlike α-Fe_2O_3 nanostructures. (c) O 1s XPS spectrum of flowerlike α-Fe_2O_3 after As^V adsorption. (d) O 1s XPS spectrum of flowerlike α-Fe_2O_3 after Cr^{VI} adsorption.

Fe−O peak after As or Cr adsorption, suggesting that hydroxyl groups have exchanged with $H_2AsO_4^-$ or $Cr_2O_7^{2-}/HCrO_4^-$ species.

The FTIR spectra of the samples after As^V and Cr^{VI} adsorption were acquired, as shown in Figure 6. The peak

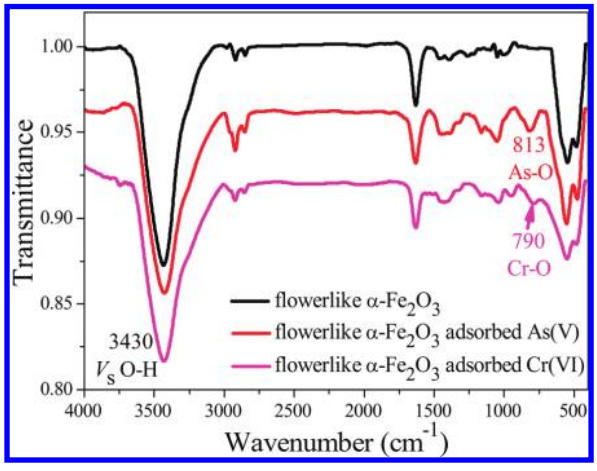

Figure 6. FTIR spectra of flowerlike α-Fe_2O_3 nanostructures before and after As^V and Cr^{VI} adsorption.

from hydroxyl groups of flowerlike α-Fe_2O_3 nanostructures at around 3430 cm^{-1} decreased after As^V and Cr^{VI} adsorption. This was consistent with XPS results. In addition, new peaks at 813 and 790 cm^{-1} appeared for flowerlike α-Fe_2O_3 nanostructures after As^V and Cr^{VI} adsorption, which can be attributed to stretching vibrations of As−O and Cr−O, respectively.[25,26]

For a better understanding of the evolution of oxygen species during adsorption, synchrotron-based XANES spectra were obtained, which provided a much higher energy resolution and, consequently, deeper insight into the adsorption processes. Figure 7 showed the normalized O K-edge XANES spectra of flowerlike α-Fe_2O_3 nanostructures before and after adsorbing heavy metal ions. All of these spectra showed a pair of well-resolved resonance peaks in the pre-edge region around 530 eV, which originated from the transitions of hybridized Fe(3d)−O(2p) states with t_{2g} and e_g orbital symmetry, respectively.[27,28] The O K-edge spectra are sensitive to the chemical environment of the oxygen atoms. In comparison to pure flowerlike α-Fe_2O_3, As^V- or Cr^{VI}-saturated samples showed a substantial decrease of the relative ratio of t_{2g} to e_g. The e_g orbital is sensitive to the ligands linked to O atoms.[29] The e_g peak intensity increased when H−O groups were replaced by $H_2AsO_4^-$ or $Cr_2O_7^{2-}/HCrO_4^-$ species, so that the ratio of t_{2g}/e_g decreased when flowerlike α-Fe_2O_3 adsorbed As^V or Cr^{VI}. On the basis of the above XPS and XANES results, we concluded that the adsorption mechanism of flowerlike α-Fe_2O_3 nanostructures for As^V and Cr^{VI} was ion exchange between hydroxyl groups and $H_2AsO_4^-$ or $Cr_2O_7^{2-}/HCrO_4^-$ species. Hydroxyl groups played critical roles for adsorption.

dx.doi.org/10.1021/la300097y | Langmuir 2012, 28, 4573−4579

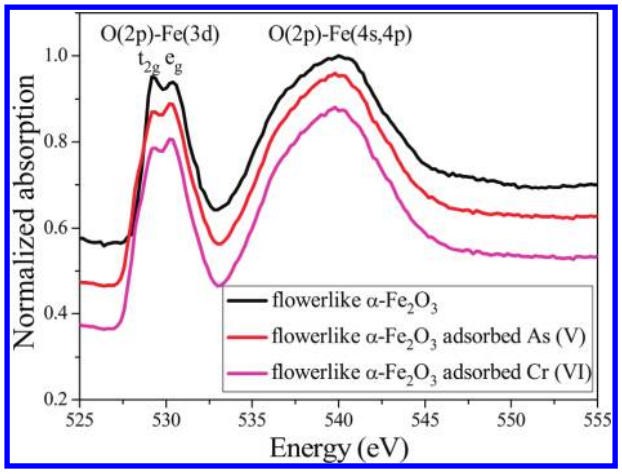

Figure 7. O K-edge XANES spectra of flowerlike α-Fe_2O_3- and flowerlike α-Fe_2O_3-adsorbed As^V and Cr^{VI} nanostructures.

4. CONCLUSION

We produced flowerlike α-Fe_2O_3 nanostructures using a low-cost template-free microwave-assisted solvothermal method. These flowerlike α-Fe_2O_3 nanostructures had a high surface area and abundant hydroxyl on the surface and showed excellent adsorption properties for As^V and Cr^{VI}. The adsorption mechanism for As^V and Cr^{VI} on flowerlike α-Fe_2O_3 nanostructures was confirmed as ion exchange between hydroxyl on the α-Fe_2O_3 surface and As^V and Cr^{VI} species. Because of the advantages, such as low cost, high surface area, and high adsorption capacity, such flowerlike α-Fe_2O_3 nanostructures were an attractive adsorbent for the removal of both As^V and Cr^{VI} from water.

■ ASSOCIATED CONTENT

Supporting Information

EDS spectrum of flowerlike α-Fe_2O_3 nanostructures (Figure S1), SEM images of samples obtained under different conditions (Figure S2), TEM images of flowerlike α-Fe_2O_3 nanostructures after As^V and Cr^{VI} adsorption (Figure S3), element mapping of flowerlike α-Fe_2O_3 after As^V and Cr^{VI} adsorption (Figure S4), and As 3d and Cr 2p XPS spectra of flowerlike α-Fe_2O_3 nanostructures after As^V and Cr^{VI} adsorption (Figure S5). This material is available free of charge via the Internet at http://pubs.acs.org.

■ AUTHOR INFORMATION

Corresponding Author

*Telephone/Fax: +86-10-62557908. E-mail: wsong@iccas.ac.cn.

Notes

The authors declare no competing financial interest.

■ ACKNOWLEDGMENTS

We thank the financial support from the National Basic Research Program of China (2009CB930400 and 2011CB933700), the National Natural Science Foundation of China (NSFC; 21121063), and the Joint Fund from the Chinese Academy of Sciences and Commonwealth Scientific and Industrial Research Organisation (CSIRO; GJHZ1224).

■ REFERENCES

(1) Yavuz, C. T.; Mayo, J. T.; Yu, W. W.; Prakash, A.; Falkner, J. C.; Yean, S.; Cong, L. L.; Shipley, H. J.; Kan, A.; Tomson, M.; Natelson, D.; Colvin, V. L. Low-field magnetic separation of monodisperse Fe_3O_4 nanocrystals. *Science* **2006**, *314*, 964.

(2) Lian, J. B.; Duan, X. C.; Ma, J. M.; Peng, P.; Kim, T. I.; Zheng, W. J. Hematite (α-Fe_2O_3) with various morphologies: Ionic liquid-assisted synthesis, formation mechanism, and properties. *ACS Nano* **2009**, *3*, 3749.

(3) Zhong, L. S.; Hu, J. S.; Liang, H. P.; Cao, A. M.; Song, W. G.; Wan, L. J. Self-assembled 3D flowerlike iron oxide nanostructures and their application in water treatment. *Adv. Mater.* **2006**, *18*, 2426.

(4) Hu, J. S.; Zhong, L. S.; Song, W. G.; Wan, L. J. Synthesis of hierarchically structured metal oxides and their application in heavy metal ion removal. *Adv. Mater.* **2008**, *20*, 2977.

(5) Li, H.; Li, W.; Zhang, Y. J.; Wang, T. S.; Wang, B.; Xu, W.; Jiang, L.; Song, W. G.; Shu, C. Y.; Wang, C. R. Chrysanthemum-like α-FeOOH microspheres produced by a simple green method and their outstanding ability in heavy metal ion removal. *J. Mater. Chem.* **2011**, *21*, 7878.

(6) Zeng, S. Y.; Tang, K. B.; Li, T. W.; Liang, Z. H.; Wang, D.; Wang, Y. K.; Qi, Y. X.; Zhou, W. W. Facile route for the fabrication of porous hematite nanoflowers: Its synthesis, growth mechanism, application in the lithium ion battery, and magnetic and photocatalytic properties. *J. Phys. Chem. C* **2008**, *112*, 4836.

(7) Hao, Q. Y.; Liu, S. A.; Yin, X. M.; Du, Z. F.; Zhang, M.; Li, L. M.; Wang, Y. G.; Wang, T. H.; Li, Q. H. Flexible morphology-controlled synthesis of mesoporous hierarchical α-Fe_2O_3 architectures and their gas-sensing properties. *CrystEngComm* **2011**, *13*, 806.

(8) Yanna, N.; Zhang, P.; Guo, Z.; Munroe, P.; Liu, H. Preparation of α-Fe_2O_3 submicro-flowers by a hydrothermal approach and their electrochemical performance in lithium-ion batteries. *Electrochim. Acta* **2008**, *53*, 4213.

(9) Yin, S. X.; Ellis, D. E. DFT studies of Cr(VI) complex adsorption on hydroxylated hematite ($1\bar{1}02$) surfaces. *Surf. Sci.* **2009**, *603*, 736.

(10) Zhong, L. S.; Hu, J. S.; Cao, A. M.; Liu, Q.; Song, W. G.; Wan, L. J. 3D flowerlike ceria micro/nanocomposite structure and its application for water treatment and Co removal. *Chem. Mater.* **2007**, *19*, 1648.

(11) Cao, C. Y.; Cui, Z. M.; Chen, C. Q.; Song, W. G.; Cai, W. Ceria hollow nanospheres produced by a template-free microwave-assisted hydrothermal method for heavy metal ion removal and catalysis. *J. Phys. Chem. C* **2010**, *114*, 9865.

(12) Bain, S. W.; Ma, Z.; Cui, Z. M.; Zhang, L. S.; Niu, F.; Song, W. G. Synthesis of micrometer-sized nanostructured magnesium oxide and its high catalytic activity in the Claisen−Schmidt condensation reaction. *J. Phys. Chem. C* **2008**, *112*, 11340.

(13) Song, W.; Justice, R. E.; Jones, C. A.; Grassian, V. H.; Larsen, S. C. Size-dependent properties of nanocrystalline silicalite synthesized with systematically varied crystal sizes. *Langmuir* **2004**, *20*, 4696.

(14) Liu, Q.; Cui, Z. M.; Ma, Z.; Bian, S. W.; Song, W. G.; Wan, L. J. Morphology control of Fe_2O_3 nanocrystals and their application in catalysis. *Nanotechnology* **2007**, 18.

(15) Berg, M.; Tran, H. C.; Nguyen, T. C.; Pham, H. V.; Schertenleib, R.; Giger, W. Arsenic contamination of groundwater and drinking water in Vietnam: A human health threat. *Environ. Sci. Technol.* **2001**, *35*, 2621.

(16) Mandal, B. K.; Suzuki, K. T. Arsenic round the world: A review. *Talanta* **2002**, *58*, 201.

(17) Mohan, D.; Pittman, C. U. Jr. Arsenic removal from water/wastewater using adsorbents—A critical review. *J. Hazard. Mater.* **2007**, *142*, 1.

(18) Vaaramaa, K.; Lehto, J. Removal of metals and anions from drinking water by ion exchange. *Desalination* **2003**, *155*, 157.

(19) Wu, Z. X.; Zhao, D. Y. Ordered mesoporous materials as adsorbents. *Chem. Commun.* **2011**, *47*, 3332.

(20) Liang, H. W.; Cao, X.; Zhang, W. J.; Lin, H. T.; Zhou, F.; Chen, L. F.; Yu, S. H. Robust and highly efficient free-standing carbonaceous

nanofiber membranes for water purification. *Adv. Funct. Mater.* **2011**, *21*, 3851.
(21) Yu, L.; Zou, R. J.; Zhang, Z. Y.; Song, G. S.; Chen, Z. G.; Yang, J. M.; Hu, J. Q. A Zn_2GeO_4-ethylenediamine hybrid nanoribbon membrane as a recyclable adsorbent for the highly efficient removal of heavy metals from contaminated water. *Chem. Commun.* **2011**, *47*, 10719.
(22) Drisko, G. L.; Luca, V.; Sizgek, E.; Scales, N.; Caruso, R. A. Template synthesis and adsorption properties of hierarchically porous zirconium titanium oxides. *Langmuir* **2009**, *25*, 5286.
(23) Li, W.; Cao, C. Y.; Wu, L. Y.; Ge, M. F.; Song, W. G. Superb fluoride and arsenic removal performance of highly ordered mesoporous aluminas. *J. Hazard. Mater.* **2011**, *198*, 143.
(24) Zhang, S.; Niu, H.; Cai, Y.; Zhao, X.; Shi, Y. Arsenite and arsenate adsorption on coprecipitated bimetal oxide magnetic nanomaterials: $MnFe_2O_4$ and $CoFe_2O_4$. *Chem. Eng. J.* **2010**, *158*, 599.
(25) Agrawal, P.; Bajpai, A. K. Dynamic column adsorption studies of toxic Cr(VI) ions onto iron oxide loaded gelatin nanoparticles. *J. Dispersion Sci. Technol.* **2011**, *32*, 1353.
(26) Pena, M.; Meng, X.; Korfiatis, G. P.; Jing, C. Adsorption mechanism of arsenic on nanocrystalline titanium dioxide. *Environ. Sci. Technol.* **2006**, *40*, 1257.
(27) Wu, Z. Y.; Gota, S.; Jollet, F.; Pollak, M.; Gautier-Soyer, M.; Natoli, C. R. Characterization of iron oxides by X-ray absorption at the oxygen K edge using a full multiple-scattering approach. *Phys. Rev. B: Condens. Matter Mater. Phys.* **1997**, *55*, 2570.
(28) Park, T. J.; Sambasivan, S.; Fischer, D. A.; Yoon, W. S.; Misewich, J. A.; Wong, S. S. Electronic structure and chemistry of iron-based metal oxide nanostructured materials: A NEXAFS investigation of $BiFeO_3$, $Bi_2Fe_4O_9$, α-Fe_2O_3, γ-Fe_2O_3, and Fe/Fe_3O_4. *J. Phys. Chem. C* **2008**, *112*, 10359.
(29) Bora, D. K.; Braun, A.; Erat, S.; Ariffin, A. K.; Löhnert, R.; Sivula, K.; Töpfer, J. r.; Grätzel, M.; Manzke, R.; Graule, T.; Constable, E. C. Evolution of an oxygen near-edge X-ray absorption fine structure transition in the upper Hubbard band in α-Fe_2O_3 upon electrochemical oxidation. *J. Phys. Chem. C* **2011**, *115*, 5619.